

Analysis and Prediction of Doppler Noise During Solar Conjunctions

A. L. Berman and S. T. Rockwell
Network Operations Office

This report presents the results of a study of doppler data noise during solar conjunctions. During the first half of 1975, a sizeable data base of doppler data noise (estimates) for the Pioneer 10, Pioneer 11, and Helios 1 solar conjunctions was accumulated. To analyze these data, certain physical assumptions are made, leading to the development of a geometric parameter ("ISI") which correlates strongly with doppler data noise under varying Sun-Earth-spacecraft geometries. Doppler noise models are then constructed from this parameter, resulting in the newfound ability to predict doppler data noise during solar conjunctions, and hence to additionally be in a position to validate doppler data acquired during solar conjunctions.

I. Introduction

During past solar conjunctions, a large increase (sometimes greater than two orders of magnitude) in doppler data noise has invariably occurred. Other than the basic observation and noting of the phenomenon, little is known about the mechanisms which result in the noise or how to predict the phenomenon for future solar conjunctions. From the standpoint of the Deep Space Network (DSN), two very cogent requirements exist which deeply underscore the need for additional study in this area, to wit:

- (1) Prediction of doppler noise so that the generation of doppler data by the tracking system during solar conjunctions can be validated.
- (2) Prediction of doppler noise for future planning of critical mission phases. As a prime example, the Pioneer 11 Saturn encounter occurs during solar conjunction, and it would be extremely useful to know the expected quality of the doppler data during the encounter.

In the past, it has frequently been assumed that high doppler noise during solar conjunctions could be accounted for by some combination of the following possible effects:

- (1) Solar radiation and/or charged particles affecting the signal during transit.
- (2) Increase in system noise temperature or other possible solar/antenna effects.

It was the authors' surmise that (1), above, was far more likely to be the predominant effect, so this was initially chosen as the direction in which this investigation of solar conjunction doppler noise would proceed.

II. Accumulation of a Solar Conjunction Doppler Noise Data Base

In early 1975, it was decided to accumulate a solar conjunction doppler noise data base for subsequent study. The first half of 1975 was a fortuitous period for collection of such data as it was during this period that Pioneers 10 and 11 underwent superior solar conjunctions, while Helios 1 underwent both inferior and superior solar conjunctions. The minimum angular separations and dates of occurrence for these events are:

- (1) Pioneer 10 superior conjunction
Date of occurrence = April 4, 1975 (DOY 094)
Minimum angular separation = 1.9 deg
- (2) Pioneer 11 superior conjunction
Date of occurrence = March 25, 1975 (DOY 084)
Minimum angular separation = 2.0 deg
- (3) Helios 1 inferior conjunction
Date of occurrence = February 19, 1975 (DOY 050)
Minimum angular separation = 0.5 deg
- (4) Helios 1 superior conjunction
Date of occurrence = May 6, 1975 (DOY 126)
Minimum angular separation = 0.4 deg

The doppler noise data were accumulated over the following intervals:

Mission	Start (DOY)	End (DOY)
Pioneer 10	064	166
Pioneer 11	061	163
Helios 1	063	166

and consist of an "average doppler noise" value for each pass (tracked) during the preceding periods. Obviously, then, each "average doppler noise" value is completely specified by three parameters:

- (1) Spacecraft
- (2) Deep Space Station (DSS)
- (3) Pass (actually date of pass)

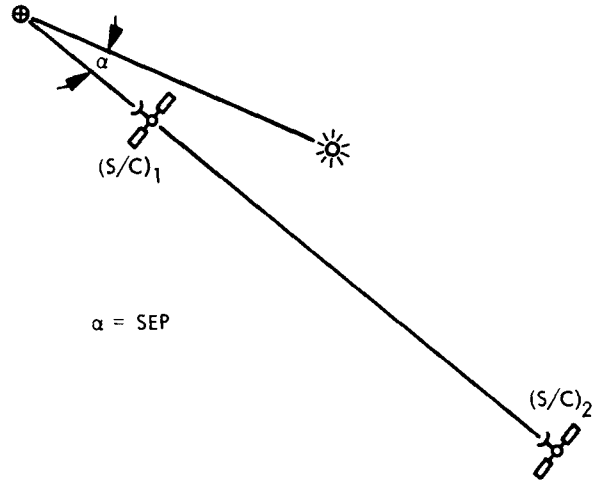
The "average doppler noise" values were obtained by manually scanning the Network Operations Control Center (NOCC) pseudoresidual output for each pass and selecting the three best (in the sense of smallest) groups of 10 to 20 values of running standard deviation (noise). The data considered were restricted to good, two-way, 60-second-sample-rate doppler data. An average value for each of the three groups was estimated and recorded, and, finally, the three group estimates were averaged to produce the "pass average." It is immediately obvious that the results obtained are the "best" (smallest noise) possible, and that one should consider that these data define the lower boundary of a band of possible noise which might be obtained on the dates the data were taken. This process was chosen because it was felt that the same process could easily be duplicated day after day, whereas any other more general averaging technique would be more difficult and less useful, because during these high noise periods, the pseudoresidual output frequently oscillates to almost meaninglessly high values.

The accumulated data comprise Tables 1, 2, and 3. Additionally, the data are plotted versus Sun-Earth-probe (SEP) angle and Earth-Sun-probe (ESP) angle in Figs. 1 through 6. The data were plotted as a function of both SEP and ESP because doppler noise is obviously a very strong function of either angle, and yet the angles, under varying Sun-Earth-spacecraft geometries, can behave (as, say, a function of time) in quite dissimilar fashions. Finally, the data in Figs. 1 through 6 are presented so that one can easily distinguish between station complexes and between 64-meter and 26-meter stations.

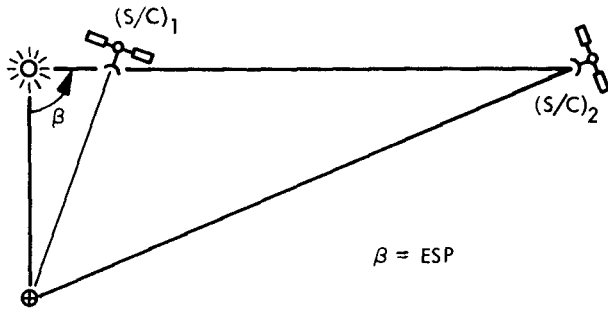
III. Consideration of Solar Effects During Signal Transit

It was originally intended to accomplish a strictly empirical fit of the collected noise data to the SEP angle or, perhaps, the ESP angle. However, it immediately strikes one that neither seems to be uniquely qualified to serve

as an independent variable. For instance, if one considers the SEP angle:



Obviously, in the above sketch, solar effects on the $(S/C)_2$ signal will be far higher than on the $(S/C)_1$ signal, and yet the spacecraft have identical SEP angles. In a similar vein, consider the ESP angle:



Equally obvious, the solar effects on the $(S/C)_1$ signal will be far higher than on the $(S/C)_2$ signal, and yet the spacecraft have identical ESP angles. It is an inescapable conclusion that neither of these angles alone, although both showing a strong functional relationship to doppler noise, is capable of serving as a reasonable independent variable for an empirical representation of doppler noise. At this point, it was felt that perhaps an elementary consideration of solar effects might shed some clues as to a more beneficial approach to the evaluation and prediction of doppler noise during solar conjunctions.

It would seem that one might expect the signal at any point to be corrupted by the solar emitted electromag-

netic field energy (flux) and/or the density of solar emitted charged particles. These two possible sources of signal corruption will be considered very briefly below, as will the conclusion to be drawn from their consideration.

A. Solar Electromagnetic Energy Flux

One can start by writing the expression for the rate of production of energy within an arbitrary finite volume:

$$\int_V \mathbf{J} \cdot \mathbf{E} dV$$

where

\mathbf{J} = current density

\mathbf{E} = electric field intensity

Now, using the Ampère/Maxwell law,

$$\nabla \times \mathbf{H} = \frac{4\pi}{c} \mathbf{J} + \frac{1}{c} \frac{\partial \mathbf{D}}{\partial t}$$

where

\mathbf{H} = magnetic field intensity

c = speed of light

\mathbf{D} = electric displacement

one obtains

$$\int_V \mathbf{J} \cdot \mathbf{E} dV = \int_V \frac{c}{4\pi} \left\{ \nabla \times \mathbf{H} - \frac{1}{c} \frac{\partial \mathbf{D}}{\partial t} \right\} \cdot \mathbf{E} dV$$

using the vector identity

$$\nabla \cdot (\mathbf{F} \times \mathbf{G}) = \mathbf{G} \cdot (\nabla \times \mathbf{F}) - \mathbf{F} \cdot (\nabla \times \mathbf{G})$$

so that

$$\nabla \cdot (\mathbf{E} \times \mathbf{H}) = \mathbf{H} \cdot (\nabla \times \mathbf{E}) - \mathbf{E} \cdot (\nabla \times \mathbf{H})$$

one would have

$$\begin{aligned} \int_V \mathbf{J} \cdot \mathbf{E} dV &= \int_V \frac{c}{4\pi} \left\{ \mathbf{H} \cdot (\nabla \times \mathbf{E}) \right. \\ &\quad \left. - \nabla \cdot (\mathbf{E} \times \mathbf{H}) - \frac{1}{c} \frac{\partial \mathbf{D}}{\partial t} \cdot \mathbf{E} \right\} dV \end{aligned}$$

By applying Faraday's law

$$\nabla \times \mathbf{E} = -\frac{1}{c} \frac{\partial \mathbf{B}}{\partial t}$$

where \mathbf{B} is the magnetic induction, one obtains

$$\begin{aligned} \int_V \mathbf{J} \cdot \mathbf{E} dV &= \int_V \frac{c}{4\pi} \left\{ -\mathbf{H} \cdot \frac{1}{c} \frac{\partial \mathbf{B}}{\partial t} \right. \\ &\quad \left. - \nabla \cdot (\mathbf{E} \times \mathbf{H}) - \frac{1}{c} \frac{\partial \mathbf{D}}{\partial t} \cdot \mathbf{E} \right\} dV \\ &= - \int_V \frac{c}{4\pi} \{ \nabla \cdot (\mathbf{E} \times \mathbf{H}) \} dV \\ &\quad + \int_V -\frac{1}{4\pi} \left\{ \mathbf{H} \cdot \frac{\partial \mathbf{B}}{\partial t} + \frac{\partial \mathbf{D}}{\partial t} \cdot \mathbf{E} \right\} dV \end{aligned}$$

since

$$\mathbf{B} = \mu \mathbf{H}$$

and

$$\mathbf{D} = \epsilon \mathbf{E}$$

where

ϵ = dielectric constant

μ = permeability constant

combined with differentiation of a vector dot product

$$\frac{\partial}{\partial t} (\mathbf{F} \cdot \mathbf{G}) = \mathbf{F} \cdot \frac{\partial \mathbf{G}}{\partial t} + \frac{\partial \mathbf{F}}{\partial t} \cdot \mathbf{G}$$

yields

$$\mathbf{H} \cdot \frac{\partial \mathbf{B}}{\partial t} + \mathbf{E} \cdot \frac{\partial \mathbf{D}}{\partial t} = \frac{1}{2} \left\{ \frac{\partial}{\partial t} [\mathbf{H} \cdot \mathbf{B} + \mathbf{E} \cdot \mathbf{D}] \right\}$$

Finally, utilizing the divergence theorem

$$\int_V \nabla \cdot \mathbf{F} dV = \oint_A \mathbf{F} \cdot d\mathbf{A}$$

or

$$\int_V \frac{c}{4\pi} \nabla \cdot (\mathbf{E} \times \mathbf{H}) dV = \oint_A \frac{c}{4\pi} (\mathbf{E} \times \mathbf{H}) \cdot d\mathbf{A}$$

one arrives at the Poynting theorem:

$$\begin{aligned} \int_V \mathbf{J} \cdot \mathbf{E} dV &= - \oint_A \frac{c}{4\pi} (\mathbf{E} \times \mathbf{H}) \cdot d\mathbf{A} \\ &\quad - \frac{\partial}{\partial t} \int_V \frac{1}{8\pi} \{ \mathbf{H} \cdot \mathbf{B} + \mathbf{E} \cdot \mathbf{D} \} dV \end{aligned}$$

The theorem basically states that the production of energy within a volume equals the time rate of change of the density of energy within a volume plus the amount of energy flux through the closed surface of the volume. The quantity of interest here is the Poynting vector (\mathbf{S}),

$$\mathbf{S} = \frac{c}{4\pi} (\mathbf{E} \times \mathbf{H}), \quad \text{in watts/meter}^2$$

where \mathbf{S} represents the energy flux at a given point. The Poynting theorem then becomes

$$\begin{aligned} \int_V \mathbf{J} \cdot \mathbf{E} dV &= - \oint_A \mathbf{S} \cdot d\mathbf{A} \\ &\quad - \frac{\partial}{\partial t} \int_V \frac{1}{8\pi} \{ \mathbf{H} \cdot \mathbf{B} + \mathbf{E} \cdot \mathbf{D} \} dV \end{aligned}$$

One can now make some assumptions which greatly simplify the expression:

- (1) *Solar Steady State.* It is assumed that solar radiation is in approximate equilibrium; hence

$$\frac{\partial}{\partial t} \int_V \frac{1}{8\pi} \{ \mathbf{H} \cdot \mathbf{B} + \mathbf{E} \cdot \mathbf{D} \} dV \approx 0$$

- (2) *Constant Production of Solar Energy.* It is assumed that the production of solar energy is approximately constant; hence

$$\int_V \mathbf{E} \cdot \mathbf{J} dV \approx -K_0$$

with the result that

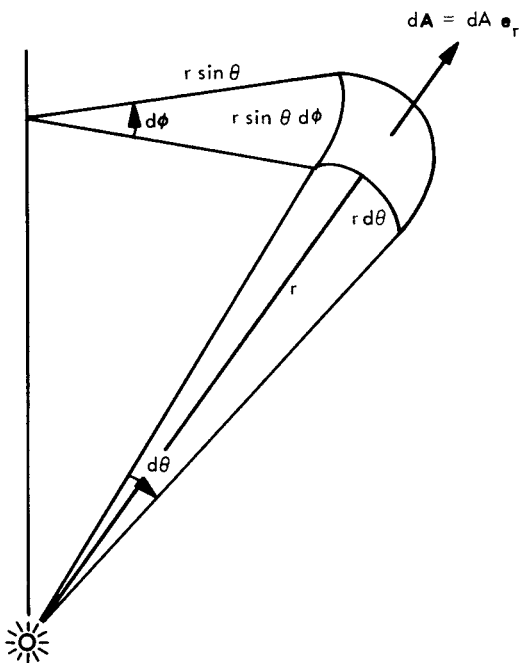
$$\oint_A \mathbf{S} \cdot d\mathbf{A} \approx K_0$$

- (3) *Spherical Uniformity of Solar Radiation.* It is assumed that solar radiation is spherically uniform, so that \mathbf{S} can only depend on the r coordinate and

can only have a component in the \mathbf{e}_r direction, i.e.,

$$\mathbf{S} = S(r) \mathbf{e}_r$$

considering a small element of surface dA



or

$$\begin{aligned} dA &= (r d\theta) (r \sin \theta d\phi) \mathbf{e}_r \\ &= r^2 \sin \theta d\theta d\phi \mathbf{e}_r \end{aligned}$$

so that

$$\begin{aligned} \oint_A \mathbf{S} \cdot d\mathbf{A} &= \int_0^{2\pi} \int_0^\pi S(r) \mathbf{e}_r \cdot r^2 \sin \theta d\theta d\phi \mathbf{e}_r \\ &= S(r) r^2 (\mathbf{e}_r \cdot \mathbf{e}_r) \int_0^{2\pi} \left[\int_0^\pi \sin \theta d\theta \right] d\phi \\ &= 2\pi S(r) r^2 \int_0^\pi \sin \theta d\theta \\ &= 4\pi S(r) r^2 \end{aligned}$$

or, finally,

$$S(r) \approx \frac{K_0}{4\pi r^2}$$

or, essentially, that solar electromagnetic radiation is proportional to $(r)^{-2}$

$$S(r) \propto \frac{1}{r^2}$$

B. Solar Emission of Charged Particles

If one could assume that charged particles are emitted spherically uniform and at a constant rate, one would define:

N = number of charged particles/second emitted by the Sun perpendicular to the surface

v_N = (uniform) particle velocity

Then, at any subsequent radius r , there will be contained in a spherical shell of volume ΔV

$$\Delta V = v_N \{4\pi r^2\} \Delta t$$

$N \Delta t$ particles, or a particle density ρ_N of

$$\rho_N \approx \frac{N \Delta t}{v_N 4\pi r^2 \Delta t} \approx \frac{N}{v_N 4\pi r^2}$$

which is just to say in a very rough sense that

$$\text{charged-particle density} \propto \frac{1}{r^2}$$

C. Final Premise for Investigation of Solar Conjunction Doppler Noise

Subsections A and B, above, indicate that the types of solar effects which might figure in the corruption of signals in transit all seem to be at least (roughly) proportional to $(r)^{-2}$. This motivates the following assumptions, which can then (possibly) be combined to construct an independent variable for correlation and prediction of solar induced doppler noise:

- (1) Assume signal corruption proportional to total length of time exposed to electromagnetic energy flux and charged particles.
- (2) Assume signal corruption proportional to intensity of electromagnetic energy flux and charged particles at any given instant.

Combining the above, let R be the path length between spacecraft and DSS. It is then hypothesized that

$$\begin{aligned} \text{Signal corruption} &\propto \int_{\text{DSS}}^{\text{S/C}} [\text{intensity}] dt \\ &= \int_0^R \left[\frac{1}{r^2} \right] \left\{ \frac{dR}{c} \right\} \end{aligned}$$

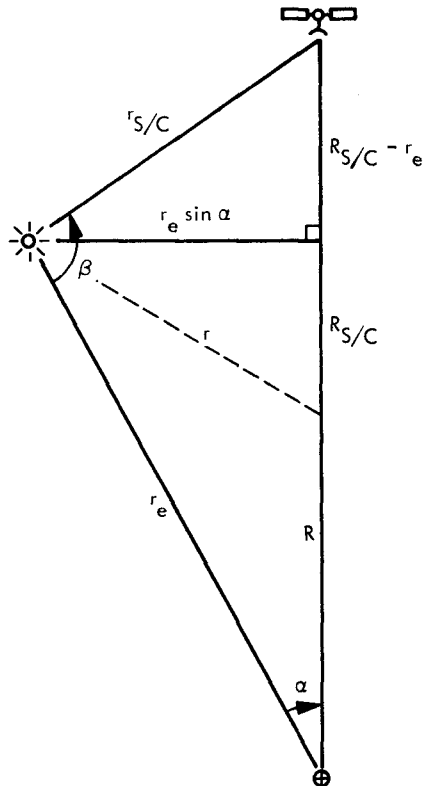
Thus a quantity ISI (integrated solar intensity) is formulated here to be

$$ISI = K \int_0^R \left(\frac{1}{r^2} \right) dR$$

where r is the distance to the Sun from any point on the signal path. If the hypothesis has any validity, then the quantity ISI might indeed be a reasonable candidate for a parametric representation of solar induced noise. The closed form solution of ISI is presented in the following section.

IV. Determination of the Parameter ISI

The Sun-Earth-spacecraft geometry can be seen in the accompanying sketch.



By the law of cosines

$$r^2 = R^2 + r_e^2 - 2Rr_e \cos \alpha$$

where

$r_{s/c}$ = spacecraft-Sun distance

r = distance from Sun to signal

R = distance along Earth-spacecraft line of sight

r_e = Earth-Sun distance

$R_{s/c}$ = Earth-spacecraft distance

α = Sun-Earth-probe angle

β = Earth-Sun-probe angle

so that

$$\begin{aligned} ISI &= K \int_0^{R_{s/c}} \frac{dR}{r^2} \\ &= K \int_0^{R_{s/c}} \frac{dR}{R^2 + r_e^2 - 2Rr_e \cos \alpha} \\ &= K \int_0^{R_{s/c}} \frac{dR}{(R^2 - 2Rr_e \cos \alpha + r_e^2 \cos^2 \alpha) + r_e^2 - r_e^2 \cos^2 \alpha} \\ &= K \int_0^{R_{s/c}} \frac{dR}{(R - r_e \cos \alpha)^2 + r_e^2(1 - \cos^2 \alpha)} \\ &= K \int_0^{R_{s/c}} \frac{dR}{(R - r_e \cos \alpha)^2 + r_e^2 \sin^2 \alpha} \end{aligned}$$

Let

$$x = R - r_e \cos \alpha$$

$$dx = dR$$

$$a = r_e \sin \alpha$$

so that

$$\begin{aligned} ISI &= K \int_{-r_e \cos \alpha}^{R_{s/c} - r_e \cos \alpha} \frac{dx}{x^2 + a^2} \\ &= \frac{K}{a^2} \int_{-r_e \cos \alpha}^{R_{s/c} - r_e \cos \alpha} \frac{dx}{\left(\frac{x^2}{a^2} + 1\right)} \end{aligned}$$

Now let

$$\frac{x}{a} = \tan w$$

$$dx = a \sec^2 w dw$$

so that

$$ISI = \frac{K}{a^2} \int_{\tan^{-1}(-r_e \cos \alpha / a)}^{\tan^{-1}(R_{s/c} - r_e \cos \alpha / a)} \frac{a \sec^2 w dw}{\tan^2 w + 1}$$

$$\begin{aligned}
&= \frac{K}{a} \int_{\tan^{-1}\left(\frac{-r_e \cos \alpha}{a}\right)}^{\tan^{-1}\left(\frac{R_{S/C} - r_e \cos \alpha}{a}\right)} dw \\
&= \frac{K}{a} \left\{ \tan^{-1}\left(\frac{R_{S/C} - r_e \cos \alpha}{a}\right) - \tan^{-1}\left(\frac{-r_e \cos \alpha}{a}\right) \right\}
\end{aligned}$$

Since $a = r_e \sin \alpha$,

$$ISI = \frac{K}{r_e \sin \alpha} \left\{ \tan^{-1}\left(\frac{R_{S/C} - r_e \cos \alpha}{r_e \sin \alpha}\right) - \tan^{-1}(-\cot \alpha) \right\}$$

and from the sketch

$$R_{S/C} - r_e \cos \alpha = r_e \sin \alpha \left[\tan\left(\beta - \left\{\frac{\pi}{2} - \alpha\right\}\right) \right]$$

combined with

$$\cot \alpha = \tan\left(\frac{\pi}{2} - \alpha\right)$$

yield

$$\begin{aligned}
ISI &= \frac{K}{r_e \sin \alpha} \left\{ \tan^{-1} \left[\tan\left(\beta - \frac{\pi}{2} + \alpha\right) \right] \right. \\
&\quad \left. - \tan^{-1} \left[-\tan\left(\frac{\pi}{2} - \alpha\right) \right] \right\} \\
&= \frac{K}{r_e \sin \alpha} \left\{ \beta - \frac{\pi}{2} + \alpha - \left(\alpha - \frac{\pi}{2} \right) \right\} \\
&= \frac{K}{r_e \sin \alpha} \{ \beta \} = \frac{K\beta}{r_e \sin \alpha}
\end{aligned}$$

K will be chosen to be

$$K = r_e \{1/\text{degrees}\}$$

so that ISI will be a unitless number when $\beta = \beta$ (degrees)

$$ISI = ISI(\alpha, \beta) = \frac{\beta}{\sin \alpha}$$

V. Correlation of ISI Versus Doppler Noise

All doppler noise data accumulated in the data base were plotted against the corresponding ISI number and can be seen in Fig. 7. It is obvious that there exists a strong correlation between observed doppler noise and ISI on a

multimission basis, and hence tends to confirm the hypothesis that ISI might represent an attractive independent variable for a doppler noise model. The hypothesis was of the form:

$$NOISE_L = C_1 \{ISI\} + C_2$$

The nominal noise (i.e., when not in solar conjunction) is considered to be approximately 0.003 Hz. Furthermore, since the correlation of doppler noise versus ISI displays a fair scatter, a reasonable set of C_1 and C_2 can be selected without the necessity of resorting to rigorous methods. The following were chosen:

$$C_1 = 3.1277 \times 10^{-5}$$

$$C_2 = -6.3831 \times 10^{-3}$$

so that the noise model $NOISE_L$ (for "linear") is defined as:

$$NOISE_L (\text{Hz}) = \begin{cases} 0.003, & ISI \leq 300 \\ C_1 \{ISI\} + C_2, & ISI > 300 \end{cases}$$

This model can be seen as plotted in Fig. 7. However, from mere observation of Fig. 7, it can be seen that a more reasonable fit to the data would be a slightly "stronger" function of ISI , say, in the form of:

$$NOISE_P = K_1 (ISI)^{1+K_2}$$

K_1 and K_2 were selected to be:

$$K_1 = 2.8 \times 10^{-6}$$

$$K_2 = 2.9 \times 10^{-1}$$

so that a noise model $NOISE_P$ (for "power") is defined as follows:

$$NOISE_P (\text{Hz}) = \begin{cases} 0.003, & ISI \leq 223 \\ K_1 (ISI)^{1+K_2}, & ISI > 223 \end{cases}$$

This model is also seen in Fig. 7.

In Figs. 8, 9, and 10, the observed doppler noise data have been plotted against ISI , and, additionally, the $NOISE_L$ and $NOISE_P$ models are included, for Pioneer 10, Pioneer 11, and Helios 1, respectively. As can be seen, the models are more reasonable for the composite doppler noise data set than they are for any of the individual

mission doppler noise data sets. These differences can be categorized as follows:

- (1) The Helios 1 observed noise data are considerably higher than the models for moderate and high *ISI*.
- (2) The Pioneer 11 observed noise data are considerably lower than the models for moderate and high *ISI*.
- (3) The Pioneer 10 observed noise data are slightly higher than the models at high *ISI*.

These differences are analyzed in detail in the following article (Ref. 1) in this Progress Report.

Tables 1, 2, and 3 present the complete data base and related *ISI* information for Pioneer 10, Pioneer 11, and Helios 1. Indicated in the tables are the following parameters:

- (1) Station (DSS)
- (2) DOY (day of year of pass)
- (3) Noise (Hz)
- (4) α (deg)
- (5) β (deg)
- (6) *ISI* (unitless)

VI. Behavior of the Quantity *ISI* for Differing Sun-Earth-Spacecraft Geometries

It is now reasonable to briefly examine the behavior of the quantity *ISI* under varying circumstances and perhaps adduce some generalities in regard to dominant characteristics displayed by *ISI* for differing Sun-Earth-spacecraft geometries.

A. Superior Conjunctions

Obviously, the major functional nature of the quantity *ISI* is almost completely determined by the quantity $(\sin \alpha)^{-1}$ as β is practically constant (~ 180 deg) when α becomes very small; hence for superior conjunctions

$$\text{Doppler noise} \propto \frac{1}{\sin \alpha}$$

B. Inferior Conjunctions

At inferior conjunctions, the *ISI* is extremely small. For instance, assume a spacecraft at 0.5 AU so that for small

α , one has

$$\alpha \approx \beta$$

and

$$ISI = \frac{\beta(\text{deg})}{\sin \alpha} = \left(\frac{180}{\pi} \right) \frac{\beta(\text{radians})}{\sin \alpha}$$

and since

$$\sin \alpha \approx \alpha \approx \beta$$

then

$$ISI \approx \frac{180}{\pi}$$

One would therefore expect no appreciable increase in doppler noise during inferior conjunctions. Helios 1 underwent inferior conjunction on February 18, 1975 and no increase in doppler noise during the period immediately surrounding February 18 was noted.

C. Helios 1 Perihelion

On March 15, 1975, Helios 1 underwent its first perihelion passage, and this represents a unique geometrical configuration to test the hypothesis from which the quantity *ISI* was generated. Over a small matter of days, while α was nearly constant ($16 \text{ deg} \lesssim \alpha \lesssim 18 \text{ deg}$), β swung from approximately 30 to 110 deg. During this interval, *ISI* became appreciable (i.e., ~ 300) when β reached approximately 85 deg. At this point, doppler noise should have begun to increase according to the proposed models, but mostly due to changing β , in sharp contrast to the more frequent superior conjunctions when almost the entire increase in doppler noise is due to changing α . Figure 11 shows the region described above, and, as predicted, the noise at $ISI \sim 300$ begins to increase, thereby lending additional confirmation to the original hypothesis from which *ISI* was derived.

D. Maximum Doppler Noise

If one considers the below conditions as lending to the maximum possible solar induced doppler noise (i.e., just prior to solar occultation),

$$\alpha \approx 0.25 \text{ deg}$$

$$\beta \approx 180 \text{ deg}$$

so that

$$ISI \approx 41,300$$

yielding

$$NOISE_L \approx 1.3 \text{ Hz}$$

$$NOISE_P \approx 2.5 \text{ Hz}$$

As a way of comparison, the highest noise recorded in this study was for Helios 1 superior conjunction:

$$\text{Doppler noise} \approx 1.7 \text{ Hz}$$

and Yip et. al., in Fig. 13 of Ref. 2, indicate a maximum obtained noise for Mariner Mars 1971 of

$$\text{Doppler noise} \approx 1.5 \text{ Hz}$$

E. Comparison to Theory

In 1970, D. O. Muhleman et. al. (Ref. 3) computed (the equivalent of) doppler noise from scintillation theory; his theoretical model is compared to $NOISE_P$ in Fig. 12. The theoretical model for all but the smallest α is far below the $NOISE_P$ model and, of course, the observed noise; however, this is not surprising as Yip et. al. (Ref. 2) made a similar observation in 1974.

In summation, the functional behavior of the quantity ISI matches the observed doppler noise at superior conjunctions, inferior conjunctions, and Helios 1 perihelion and, hence, tends to strengthen confidence in the original hypothesis and the derivative models.

VII. Summary

During early 1975, a large data base of doppler noise data was accumulated for the solar conjunctions of Pioneer 10, Pioneer 11, and Helios 1. In analyzing these

data, certain elementary physical assumptions about the nature of solar-induced corruption of doppler data were made, with the result being the development of a parameter " ISI " which is solely dependent on a given Sun-Earth-spacecraft geometry, viz:

$$ISI(\alpha, \beta) = \frac{\beta}{\sin \alpha}$$

where

α = Sun-Earth-probe angle

β = Earth-Sun-probe angle

This parameter is shown to correlate strongly with observed doppler noise on a multimission basis, and, additionally, functionally matches observed doppler noise for three radically different types of Earth-Sun-spacecraft geometries:

- (1) Superior solar conjunctions
- (2) Inferior solar conjunctions
- (3) Helios 1 perihelion

Using the parameter ISI , a noise model ($NOISE_P$) is presented for operations usage:

$$NOISE_P(\text{Hz}) = \begin{cases} 0.003, & ISI \leq 223 \\ K_1(ISI)^{1+K_2}, & ISI > 223 \end{cases}$$

where

$$K_1 = 2.8 \times 10^{-6}$$

$$K_2 = 2.9 \times 10^{-1}$$

The above model should allow for preplanning of critical mission phases which intersect solar conjunctions and also for routine validation of doppler data quality and tracking system performance during solar conjunctions.

Acknowledgment

The authors would like to acknowledge Larry E. Bright for technical consultation, M. Leung for collection of the data, and M. F. Cates for the very fine graphical illustrations.

References

1. Berman, A. L., and Rockwell, S. T., "Correlation of Doppler Noise During Solar Conjunctions With Fluctuations in Solar Activity," in *The Deep Space Network Progress Report 42-30* (this volume), Jet Propulsion Laboratory, Pasadena, Calif., Dec. 15, 1975.
2. Yip, K. W., Winn, F. B., and Reinbold, S. J., "DSN-MVM'73 S/X Dual-Frequency Doppler Demonstration During Superior Conjunction," in *The Deep Space Network Progress Report 42-25*, pp. 47-55, Jet Propulsion Laboratory, Pasadena, Calif., Feb. 15, 1975.
3. Muhleman, D. O., Anderson, J. D., Esposito, P. B., and Martin, W. L., "Radio Propagation Measurements of the Solar Corona and Gravitational Field; Applications to Mariner 6 and 7," in *Proceedings of the Conference on Experimental Tests of Gravitational Theories*, California Institute of Technology, Pasadena, Calif., Nov. 1970.

Table 1. Pioneer 10 solar conjunction, 1975

Deep Space Station (DSS)	Day of year (DOY)	Average doppler noise, Hz	Sun-Earth-probe angle α , deg	Earth-Sun-probe angle β , deg	Integrated solar intensity (ISI)
11	65	0.0076	23.18	153.58	390
11	66	0.0078	22.34	154.50	406
11	67	0.0102	21.52	155.42	424
11	70	0.0121	19.11	158.17	483
11	72	0.0173	17.50	160.00	532
11	74	0.0120	15.90	161.83	591
11	77	0.0115	13.51	164.56	705
11	78	0.0139	12.71	165.47	752
11	79	0.0147	11.92	166.38	806
11	80	0.0151	11.13	167.28	867
11	82	0.0221	9.55	169.08	1019
11	83	0.0407	8.77	169.98	1115
11	109	0.0213	12.28	166.00	781
11	110	0.0173	13.07	165.11	730
12	76	0.0139	14.30	163.65	662
14	88	0.1240	4.94	174.35	2025
14	89	0.1900	4.21	175.19	2386
14	90	0.1173	3.51	175.98	2874
14	91	0.0950	2.87	176.72	3529
14	117	0.0054	18.59	158.84	498
14	128	0.0117	27.34	148.98	324
14	130	0.0073	28.94	147.20	304
14	131	0.0045	29.74	146.30	295
14	138	0.0069	35.35	140.05	242
14	140	0.0034	36.97	138.26	230
14	142	0.0056	38.58	136.48	219
14	144	0.0041	40.20	134.70	209
14	145	0.0037	41.01	133.81	204
14	146	0.0029	41.82	132.91	199
14	149	0.0038	44.25	130.24	187
14	150	0.0040	45.07	129.35	183
14	151	0.0032	45.88	128.46	179
14	161	0.0036	54.11	119.56	148
42	64	0.0051	23.94	152.66	376
42	65	0.0122	23.18	153.58	390
42	68	0.0081	20.72	156.34	442
42	70	0.0138	19.11	158.17	483
42	71	0.0128	18.30	159.09	507
42	136	0.0174	33.75	141.83	255
42	137	0.0075	34.55	140.94	249
42	139	0.0112	36.16	139.15	236
43	84	0.0385	7.99	170.87	1229
43	85	0.0345	7.21	171.75	1368
43	89	0.1167	4.21	175.19	2386

Table 1 (contd)

Deep Space Station (DSS)	Day of year (DOY)	Average doppler noise, Hz	Sun-Earth-probe angle α , deg	Earth-Sun-probe angle β , deg	Integrated solar intensity (ISI)
43	98	0.0647	3.87	175.58	2602
43	99	0.0545	4.58	174.77	2189
43	100	0.0393	5.38	173.93	1856
43	104	0.0343	8.37	170.45	1171
43	106	0.0208	9.93	168.67	978
43	108	0.0297	11.49	166.89	838
43	109	0.0163	12.28	166.00	781
43	111	0.0132	13.85	164.21	686
43	112	0.0096	14.64	163.32	646
43	113	0.0059	15.43	162.42	610
43	114	0.0049	16.22	161.53	578
43	115	0.0050	17.01	160.63	549
43	118	0.0052	19.38	157.94	476
43	120	0.0042	20.97	156.15	436
43	121	0.0097	21.77	155.25	419
43	122	0.0053	22.56	154.36	402
43	124	0.0066	24.15	152.57	373
43	159	0.0032	52.45	121.34	153
43	160	0.0034	53.28	120.45	150
43	161	0.0039	54.11	119.56	148
43	162	0.0038	54.93	118.67	145
44	74	0.0183	15.90	161.83	591
44	77	0.0147	13.51	164.56	705
44	80	0.0298	11.13	167.28	867
44	81	0.0157	10.34	168.18	937
44	120	0.0118	20.97	156.15	436
61	64	0.0083	23.94	152.66	376
61	66	0.0055	22.34	154.50	406
61	72	0.0160	17.50	160.00	532
61	83	0.0323	8.77	169.98	1115
61	135	0.0120	32.94	142.73	262
61	149	0.0110	44.25	130.24	187
62	147	0.0032	42.63	132.02	195
63	70	0.0082	19.11	158.17	483
63	74	0.0108	15.90	161.83	591
63	81	0.0089	10.34	168.18	937
63	85	0.0291	7.21	171.75	1368
63	86	0.0670	6.45	172.63	1538
63	87	0.0813	5.69	173.50	1751
63	88	0.0950	4.94	174.35	2025
63	89	0.0950	4.21	175.19	2386
63	90	0.0960	3.51	175.98	2874
63	91	0.1490	2.87	176.72	3529

Table 1 (contd)

Deep Space Station (DSS)	Day of year (DOY)	Average doppler noise, Hz	Sun-Earth-probe angle α , deg	Earth-Sun-probe angle β , deg	Integrated solar intensity (ISI)
63	92	0.1570	2.33	177.34	4362
63	94	0.1703	1.90	177.83	5364
63	99	0.0615	4.58	174.77	2189
63	100	0.0487	5.38	173.93	1856
63	101	0.0413	6.09	173.07	1632
63	102	0.0391	6.83	172.20	1448
63	105	0.0232	9.15	169.56	1067
63	106	0.0236	9.93	168.67	978
63	107	0.0236	10.71	167.78	903
63	108	0.0214	11.49	166.89	838
63	109	0.0225	12.28	166.00	781
63	110	0.0159	13.07	165.11	730
63	111	0.0099	13.85	164.21	686
63	112	0.0082	14.64	163.32	646
63	113	0.0061	15.43	162.42	610
63	115	0.0048	17.01	160.63	549
63	116	0.0046	17.80	159.73	523
63	117	0.0043	18.59	158.84	498
63	118	0.0046	19.38	157.94	476
63	120	0.0033	20.97	156.15	436
63	121	0.0099	21.77	155.25	419
63	122	0.0066	22.56	154.36	402
63	123	0.0049	23.35	153.46	387
63	124	0.0046	24.15	152.57	373
63	125	0.0091	24.95	151.67	360
63	126	0.0063	25.74	150.78	347
63	127	0.0096	26.54	149.88	335
63	128	0.0076	27.34	148.98	324
63	130	0.0096	28.94	147.20	304
63	131	0.0079	29.74	146.30	295
63	132	0.0072	30.54	145.41	286
63	133	0.0046	31.34	144.51	278
63	134	0.0103	32.14	143.62	270
63	136	0.0154	33.75	141.83	255
63	137	0.0065	34.55	140.94	249
63	138	0.0054	35.35	140.05	242
63	139	0.0049	36.16	139.15	236
63	140	0.0030	36.97	138.26	230
63	141	0.0030	37.77	137.37	224
63	143	0.0031	39.39	135.59	214
63	144	0.0028	40.20	134.70	209
63	145	0.0027	41.01	133.81	204
63	148	0.0031	43.44	131.13	191
63	150	0.0032	45.07	129.35	183
63	151	0.0025	45.88	128.46	179
63	152	0.0031	46.70	127.57	175
63	153	0.0037	47.52	126.68	172

Table 1 (contd)

Deep Space Station (DSS)	Day of year (DOY)	Average doppler noise, Hz	Sun-Earth-probe angle α , deg	Earth-Sun-probe angle β , deg	Integrated solar intensity (ISI)
63	154	0.0030	48.34	125.79	168
63	156	0.0027	49.98	124.01	162
63	157	0.0024	50.80	123.12	159
63	158	0.0028	51.63	122.23	156
63	159	0.0025	52.45	121.34	153
63	161	0.0027	54.11	119.56	148
63	162	0.0031	54.93	118.67	145
63	163	0.0040	55.76	117.79	142
63	164	0.0033	56.60	116.90	140
63	165	0.0029	57.43	116.01	138

Table 2. Pioneer 11 solar conjunction, 1975

Deep Space Station (DSS)	Day of year (DOY)	Average doppler noise, Hz	Sun-Earth probe angle α , deg	Earth-Sun-probe angle β , deg	Integrated solar intensity (ISI)
11	76	0.0235	5.22	173.63	1905
11	87	0.0350	3.56	175.64	2829
11	89	0.0227	4.80	174.12	2081
11	90	0.0203	5.45	173.33	1825
11	91	0.0255	6.11	172.51	1621
11	92	0.0230	6.78	171.69	1454
11	93	0.0211	7.45	170.87	1318
11	94	0.0200	8.13	170.03	1203
11	95	0.0139	8.81	169.20	1105
11	98	0.0196	10.86	166.68	885
11	103	0.0116	14.29	162.46	658
12	61	0.0170	15.84	160.75	589
12	64	0.0111	13.66	163.38	692
12	66	0.0187	12.22	165.12	780
12	67	0.0172	11.50	165.99	833
12	69	0.0223	10.07	167.72	959
12	70	0.0216	9.36	168.58	1037
12	71	0.0218	8.66	169.44	1125
12	72	0.0473	7.95	170.29	1231
12	74	0.0307	6.57	171.98	1503
12	100	0.0165	12.23	164.99	779
12	104	0.0122	14.98	161.62	625
12	108	0.0112	17.73	158.25	520
12	109	0.0172	18.41	157.40	498
12	110	0.0088	19.10	156.56	478
12	111	0.0078	19.79	155.72	460
12	112	0.0119	20.47	154.88	443
12	113	0.0043	21.16	154.04	427
12	114	0.0033	21.84	153.20	412
12	115	0.0034	22.53	152.36	398
12	116	0.0037	23.21	151.53	384
12	117	0.0033	23.90	150.69	372
12	119	0.0038	25.27	149.01	349
12	122	0.0040	27.32	146.51	319
12	123	0.0046	28.00	145.67	310
12	124	0.0041	28.69	144.84	302
12	125	0.0071	29.37	144.01	294
12	126	0.0051	30.05	143.17	286
12	127	0.0080	30.74	142.34	278
12	129	0.0056	32.11	140.68	265
12	130	0.0039	32.89	139.85	258
12	131	0.0057	33.48	139.02	252
12	132	0.0069	34.16	138.19	246
12	135	0.0083	36.22	135.71	230
12	136	0.0077	36.90	134.89	225
12	137	0.0032	37.59	134.06	220

Table 2 (contd)

Deep Space Station (DSS)	Day of year (DOY)	Average doppler noise, Hz	Sun-Earth probe angle α , deg	Earth-Sun-probe angle β , deg	Integrated solar intensity (ISI)
12	138	0.0044	38.27	133.24	215
12	139	0.0047	38.96	132.41	211
12	140	0.0053	39.64	131.59	206
12	144	0.0025	42.39	128.30	190
12	145	0.0033	43.07	127.49	187
12	146	0.0029	43.76	126.67	183
12	147	0.0035	44.45	125.85	180
12	148	0.0034	45.14	125.03	176
12	149	0.0029	45.83	124.21	173
12	150	0.0030	46.52	123.40	170
12	151	0.0026	47.21	122.58	167
12	152	0.0054	47.90	121.76	164
12	153	0.0031	48.59	120.95	161
12	154	0.0044	49.28	120.13	159
12	155	0.0028	49.98	119.32	156
12	156	0.0027	50.67	118.51	153
12	158	0.0026	52.06	116.88	148
12	159	0.0025	52.76	116.07	146
12	160	0.0026	53.45	115.25	143
12	161	0.0024	54.15	114.44	141
12	162	0.0044	54.85	113.63	139
12	163	0.0051	55.55	112.82	137
14	82	0.1217	2.04	177.50	4986
14	83	0.0973	1.97	177.58	5166
14	85	0.0573	2.51	176.93	4040
14	129	0.0053	32.11	140.68	265
14	157	0.0025	51.36	117.69	151
42	82	0.1583	2.04	177.50	4986
42	135	0.0050	36.22	135.71	230
42	140	0.0032	39.64	131.59	206
42	148	0.0031	45.14	125.03	176
42	158	0.0023	52.06	116.88	148
43	88	0.0343	4.17	174.90	2405
43	102	0.0143	13.61	163.31	694
43	103	0.0125	14.29	162.46	658
43	107	0.0127	17.04	159.09	543
43	120	0.0087	25.95	148.18	339
44	65	0.0175	12.94	164.25	733
44	66	0.0145	12.22	165.12	780
44	67	0.0206	11.50	165.99	833
44	69	0.0225	10.07	167.72	959
44	70	0.0252	9.36	168.58	1037
44	73	0.0338	7.26	171.14	1354

Table 2 (contd)

Deep Space Station (DSS)	Day of year (DOY)	Average doppler noise, Hz	Sun-Earth probe angle α , deg	Earth-Sun-probe angle β , deg	Integrated solar intensity (ISI)
44	75	0.0285	5.89	172.81	1684
44	89	0.0403	4.80	174.12	2081
44	90	0.0230	5.45	173.33	1825
44	96	0.0152	9.49	168.36	1021
44	98	0.0150	10.86	166.68	885
44	99	0.0148	11.55	165.84	828
44	100	0.0258	12.23	164.99	779
44	104	0.0139	14.98	161.62	625
44	105	0.0111	15.67	160.78	595
44	106	0.0136	16.35	159.93	568
44	108	0.0132	17.73	158.25	520
44	109	0.0153	18.41	157.40	498
44	110	0.0097	19.10	156.56	478
44	111	0.0063	19.79	155.72	460
44	112	0.0075	20.47	154.88	443
44	113	0.0041	21.16	154.04	427
44	114	0.0053	21.84	153.20	412
44	115	0.0050	22.53	152.36	398
44	116	0.0049	23.21	151.53	384
44	117	0.0048	23.90	150.69	372
44	118	0.0045	24.58	149.85	360
44	119	0.0052	25.27	149.01	349
44	121	0.0064	26.63	147.34	329
44	122	0.0058	27.32	146.51	319
44	123	0.0049	28.00	145.67	310
44	136	0.0084	36.90	134.89	225
44	137	0.0045	37.59	134.06	220
44	138	0.0040	38.27	133.24	215
44	139	0.0055	38.96	132.41	211
44	141	0.0037	40.33	130.77	202
44	143	0.0036	41.70	129.12	194
44	144	0.0034	42.39	128.30	190
44	145	0.0040	43.07	127.49	187
44	146	0.0037	43.76	126.67	183
44	147	0.0041	44.45	125.85	180
44	149	0.0043	45.83	124.21	173
44	150	0.0046	46.52	123.40	170
44	151	0.0038	47.21	122.58	167
44	152	0.0047	47.90	121.76	164
44	153	0.0052	48.59	120.95	161
44	154	0.0059	49.28	120.13	159
44	155	0.0053	49.98	119.32	156
44	156	0.0044	50.67	118.51	153
44	157	0.0049	51.36	117.69	151
44	159	0.0042	52.76	116.07	146
44	160	0.0032	53.45	115.25	143
44	161	0.0044	54.15	114.44	141
44	162	0.0044	54.85	113.63	139

Table 2 (contd)

Deep Space Station (DSS)	Day of year (DOY)	Average doppler noise, Hz	Sun-Earth probe angle α , deg	Earth-Sun-probe angle β , deg	Integrated solar intensity (ISI)
61	63	0.0075	14.38	162.51	654
61	64	0.0124	13.66	163.38	692
61	65	0.0142	12.94	164.25	733
61	68	0.0215	10.78	166.86	892
61	70	0.0280	9.36	168.58	1037
61	72	0.0333	7.95	170.29	1231
61	73	0.0275	7.26	171.14	1354
61	74	0.0278	6.57	171.98	1503
61	75	0.0467	5.89	172.81	1684
61	88	0.0340	4.17	174.90	2405
61	89	0.0207	4.80	174.12	2081
61	90	0.0243	5.45	173.33	1825
61	91	0.0208	6.11	172.51	1621
61	92	0.0237	6.78	171.69	1454
61	94	0.0260	8.13	170.03	1203
61	95	0.0155	8.81	169.20	1105
61	97	0.0163	10.17	167.52	949
61	98	0.0177	10.86	166.68	885
61	99	0.0201	11.55	165.84	828
61	100	0.0136	12.23	164.99	779
61	101	0.0129	12.92	164.15	734
61	102	0.0164	13.61	163.31	694
61	104	0.0125	14.98	161.62	625
61	105	0.0129	15.67	160.78	595
61	106	0.0107	16.35	159.93	568
61	107	0.0088	17.04	159.09	543
61	108	0.0125	17.73	158.25	520
61	109	0.0117	18.41	157.40	498
61	110	0.0124	19.10	156.56	478
61	111	0.0080	19.79	155.72	460
61	112	0.0065	20.47	154.88	443
61	113	0.0048	21.16	154.04	427
61	114	0.0035	21.84	153.20	412
61	118	0.0041	24.58	149.85	360
61	119	0.0036	25.27	149.01	349
61	120	0.0038	25.95	148.18	339
61	129	0.0053	32.11	140.68	265
61	130	0.0052	32.89	139.85	258
61	132	0.0062	34.16	138.19	246
61	133	0.0033	34.85	137.37	240
61	137	0.0064	37.59	134.06	220
61	138	0.0038	38.27	133.24	215
61	139	0.0040	38.96	132.41	211
61	140	0.0032	39.64	131.59	206
61	141	0.0032	40.33	130.77	202
61	145	0.0026	43.07	127.49	187
61	151	0.0032	47.21	122.58	167

Table 2 (contd)

Deep Space Station (DSS)	Day of year (DOY)	Average doppler noise, Hz	Sun-Earth probe angle α , deg	Earth-Sun-probe angle β , deg	Integrated solar intensity (ISI)
61	152	0.0028	47.90	121.76	164
61	153	0.0034	48.59	120.95	161
61	158	0.0025	52.06	116.88	148
61	162	0.0029	54.85	113.63	139
61	163	0.0035	55.55	112.82	137
62	117	0.0051	23.90	150.69	372
62	121	0.0044	26.63	147.34	329
62	122	0.0077	27.32	146.51	319
62	123	0.0046	28.00	145.67	310
62	124	0.0045	28.69	144.84	302
62	125	0.0051	29.37	144.01	294
62	126	0.0071	30.05	143.17	286
62	127	0.0078	30.74	142.34	278
62	128	0.0067	31.42	141.51	271
62	131	0.0059	33.48	139.02	252
62	133	0.0087	34.85	137.37	240
62	135	0.0041	36.22	135.71	230
62	136	0.0123	36.90	134.89	225
62	142	0.0032	41.01	129.95	198
62	143	0.0036	41.70	129.12	194
62	146	0.0032	43.76	126.67	183
62	147	0.0034	44.45	125.85	180
62	148	0.0032	45.14	125.03	176
62	149	0.0037	45.83	124.21	173
62	150	0.0036	46.52	123.40	170
62	154	0.0038	49.28	120.13	159
62	155	0.0037	49.98	119.32	156
62	156	0.0031	50.67	118.51	153
62	159	0.0029	52.76	116.07	146
62	160	0.0032	53.45	115.25	143
62	161	0.0031	54.15	114.44	141
63	77	0.0326	4.56	174.43	2194
63	78	0.0587	3.93	175.20	2556
63	79	0.0550	3.33	175.93	3029
63	80	0.0540	2.78	176.60	3641
63	82	0.0850	2.04	177.50	4986
63	83	0.1060	1.97	177.58	5166
63	84	0.0613	2.14	177.38	4750
63	85	0.0737	2.51	176.93	4040
63	86	0.0490	3.00	176.33	3369
63	155	0.0028	49.98	119.32	156

Table 3. Helios 1 solar conjunction, 1975

Deep Space Station (DSS)	Day of year (DOY)	Average doppler noise, Hz	Sun-Earth probe angle α , deg	Earth-Sun-probe angle β , deg	Integrated solar intensity (ISI)
12	63	0.0041	16.21	29.90	107
12	75	0.0050	17.17	91.94	311
12	79	0.0197	14.89	114.51	446
12	88	0.0109	9.18	149.12	935
12	89	0.0099	8.61	151.68	1013
12	90	0.0112	8.07	154.03	1097
12	91	0.0198	7.56	156.19	1187
12	92	0.0253	7.06	158.19	1287
12	93	0.0255	6.59	160.03	1394
12	94	0.0727	6.14	161.73	1512
12	95	0.0527	5.71	163.29	1641
12	98	0.1293	4.55	167.28	2109
12	99	0.0790	3.57	170.41	2737
12	101	0.1153	4.21	168.41	2294
12	102	0.2017	3.28	171.30	2994
14	64	0.0044	16.84	33.62	116
14	65	0.0033	17.37	37.64	126
14	66	0.0054	17.80	41.96	137
14	67	0.0031	18.14	46.59	150
14	69	0.0057	18.49	56.74	179
14	70	0.0063	18.51	62.23	196
14	73	0.0037	17.97	79.85	259
14	74	0.0053	17.61	85.91	284
14	76	0.0074	16.67	97.87	341
14	77	0.0118	16.11	103.64	374
14	78	0.0132	15.52	109.20	408
14	81	0.0164	13.59	124.24	529
14	83	0.0211	12.27	132.76	625
14	84	0.0190	11.62	136.57	678
14	85	0.0177	10.98	140.09	736
14	86	0.0103	10.36	143.35	797
14	96	0.0631	5.30	164.73	1783
14	97	0.1460	4.92	166.06	1936
14	100	0.1210	3.88	169.45	2504
14	103	0.2000	3.01	172.11	3278
14	104	0.2783	2.76	172.86	3590
14	109	0.5433	1.72	175.76	5856
14	110	0.7050	1.56	176.20	6472
14	111	0.4893	1.41	176.60	7177
14	112	0.5500	1.27	176.96	7984
14	113	0.5133	1.14	177.28	8911
14	114	0.8800	1.03	177.57	9878
14	115	0.8367	0.92	177.83	11075
14	117	1.7333	0.75	178.26	13618
14	138	1.5933	0.91	178.09	11213
14	150	0.3583	2.01	175.86	5014
14	166	0.1267	3.96	171.96	2490

Table 3 (contd)

Deep Space Station (DSS)	Day of year (DOY)	Average doppler noise, Hz	Sun-Earth probe angle α , deg	Earth-Sun-probe angle β , deg	Integrated solar intensity (ISI)
42	84	0.0252	11.62	136.57	678
42	88	0.0133	9.18	149.12	935
42	89	0.0108	8.61	151.68	1013
42	90	0.0127	8.07	154.03	1097
42	98	0.0793	4.55	167.28	2109
42	99	0.0823	4.21	168.41	2294
42	100	0.0790	3.88	169.45	2504
42	101	0.1150	3.57	170.41	2737
42	150	0.4283	2.01	175.86	5014
42	154	0.2300	2.47	174.94	4059
43	63	0.0049	16.21	29.90	107
43	65	0.0048	17.37	37.64	126
43	66	0.0052	17.80	41.96	137
43	67	0.0033	18.14	46.59	150
43	69	0.0046	18.49	56.74	179
43	70	0.0051	18.51	62.23	196
43	73	0.0039	17.97	79.85	259
43	80	0.0134	14.24	119.52	486
43	81	0.0148	13.59	124.24	529
43	83	0.0248	12.27	132.76	625
43	84	0.0161	11.62	136.57	678
43	85	0.0157	10.98	140.09	736
43	86	0.0129	10.36	143.35	797
43	96	0.0385	5.30	164.73	1783
44	92	0.0313	7.06	158.19	1287
44	93	0.0387	6.59	160.03	1394
44	94	0.0565	6.14	161.73	1512
44	95	0.0451	5.71	163.29	1641
44	97	0.0893	4.92	166.06	1936
44	103	0.2083	3.01	172.11	3278
62	64	0.0072	16.84	33.62	116
62	65	0.0036	17.37	37.64	126
62	72	0.0032	18.25	73.84	236
62	73	0.0068	17.97	79.85	259
62	76	0.0081	16.67	97.87	341
62	79	0.0230	14.89	114.51	446
62	86	0.0137	10.36	143.35	797
62	93	0.0723	6.59	160.03	1394
62	100	0.0707	3.88	169.45	2504

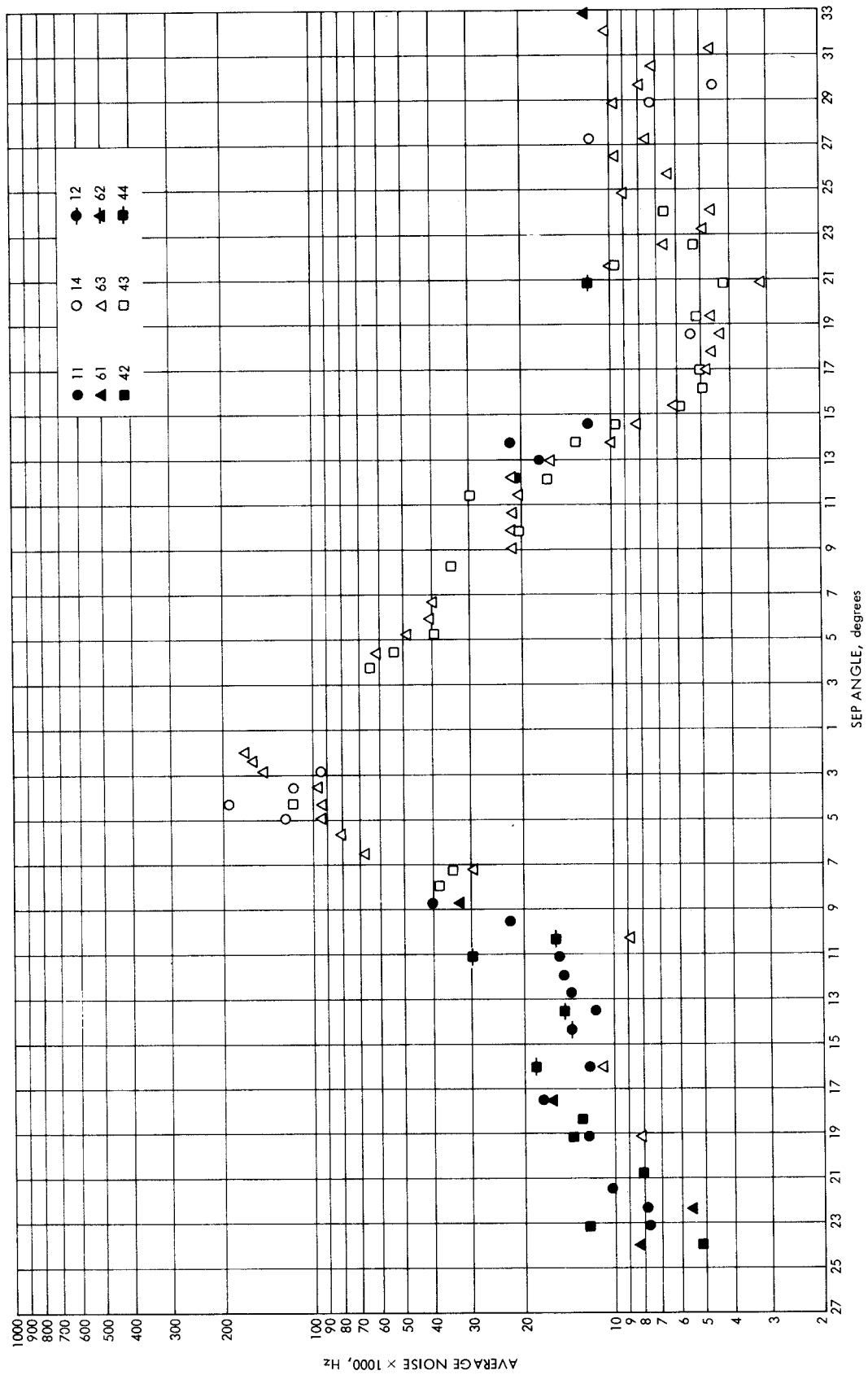


Fig. 1. Pioneer 10 average noise vs SEP angle

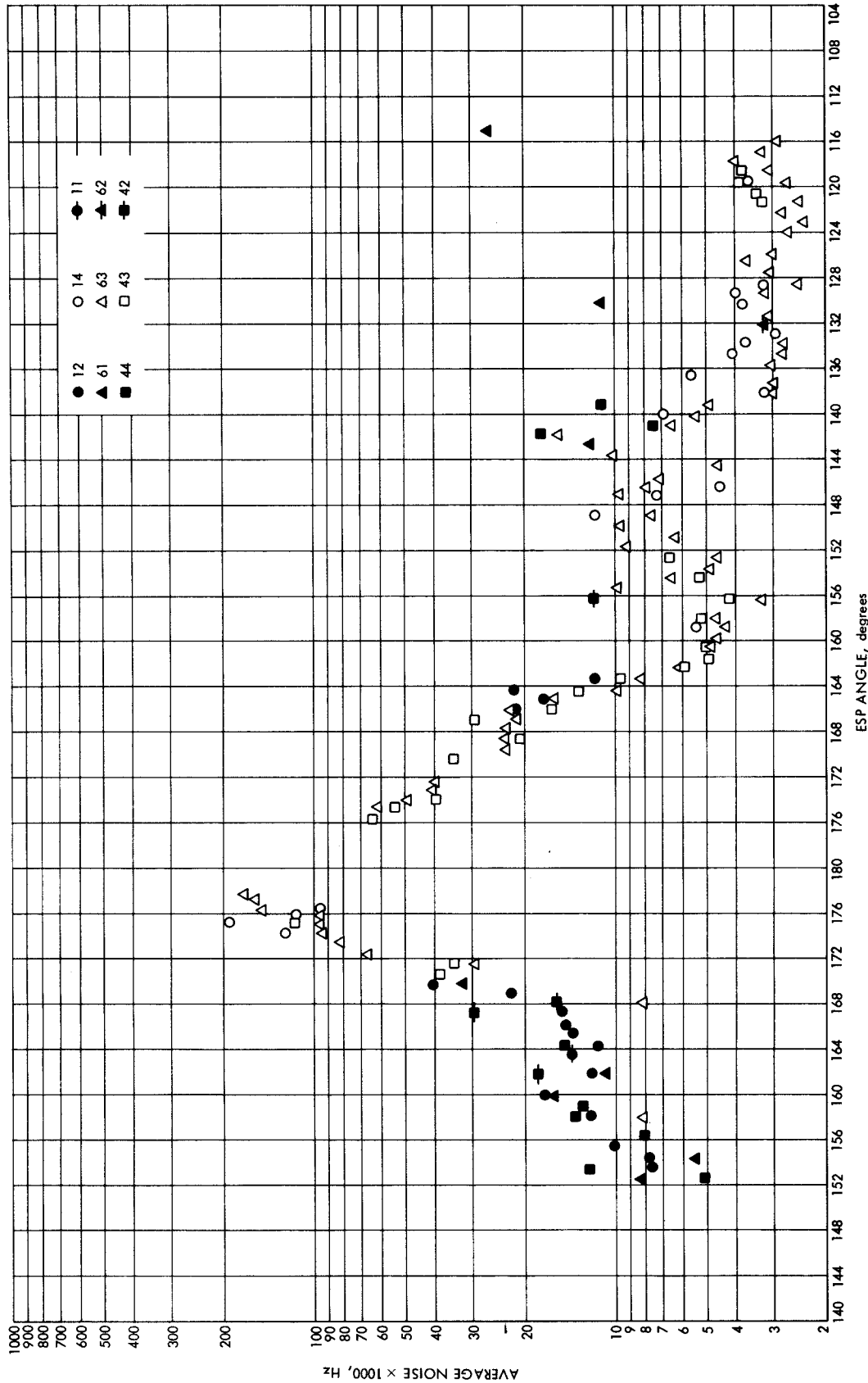


Fig. 2. Pioneer 10 average noise vs ESP angle

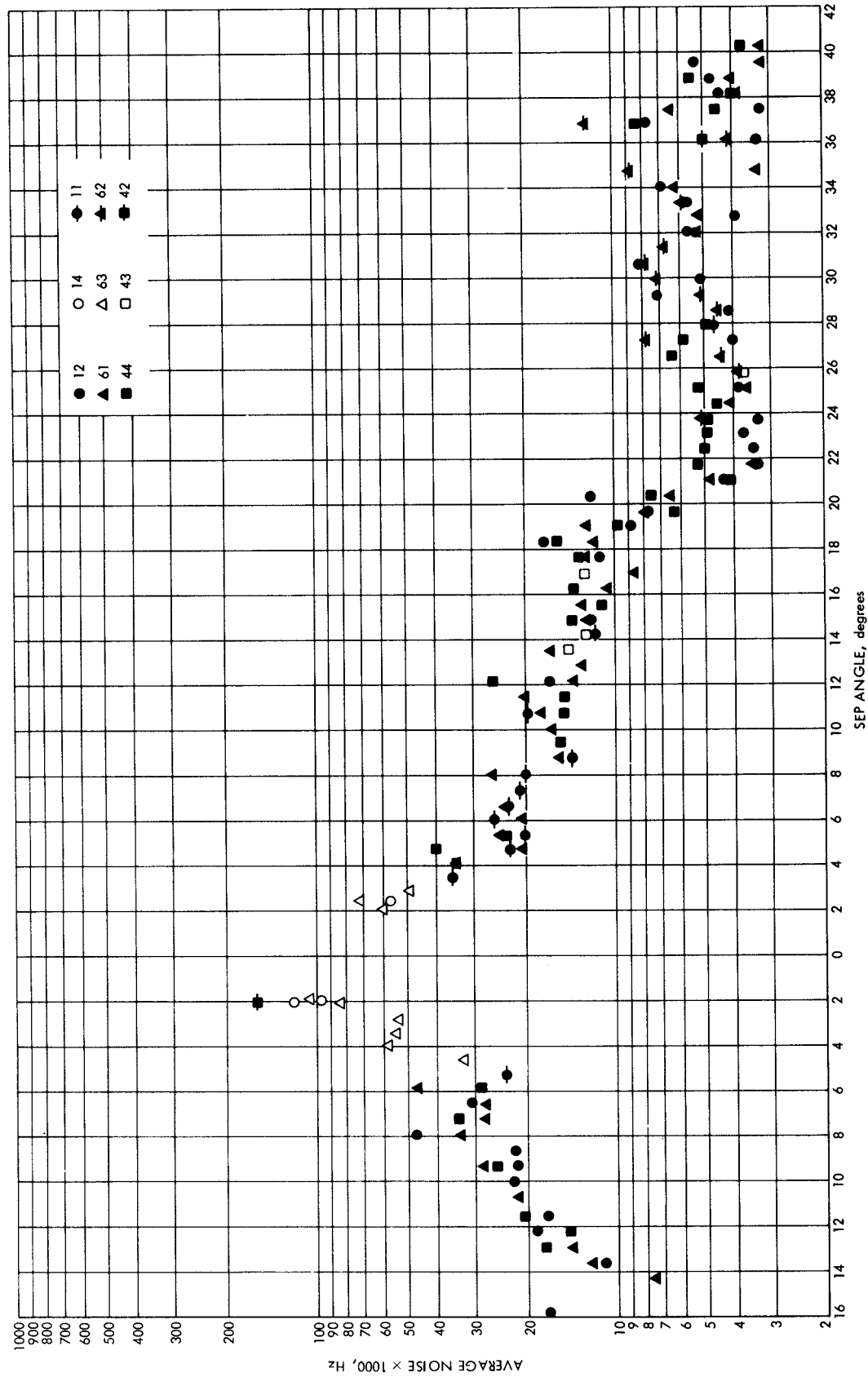


Fig. 3. Pioneer 11 average noise vs SEP angle

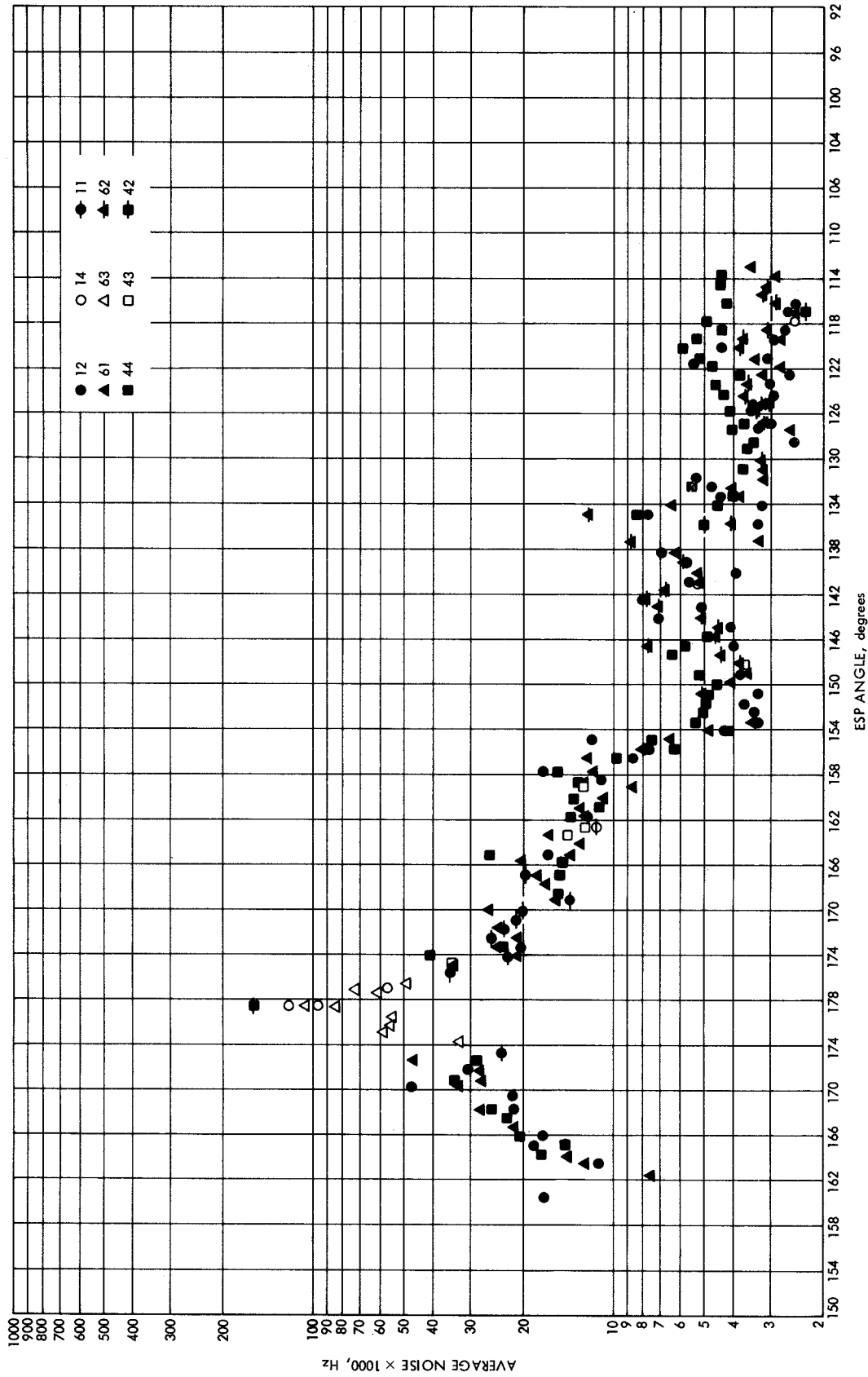


Fig. 4. Pioneer 11 average noise vs ESP angle

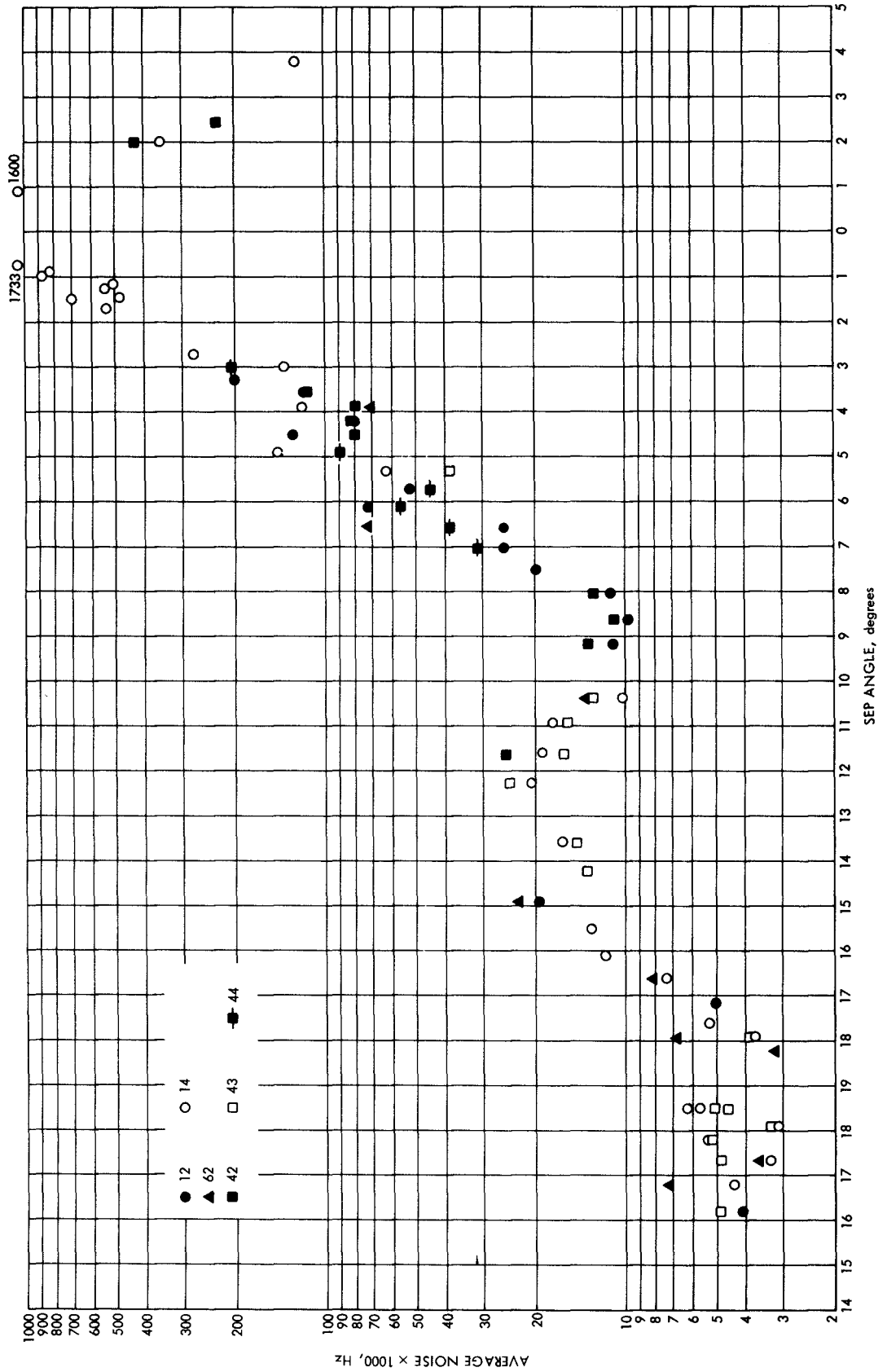


Fig. 5. Helios 1 average noise vs SEP angle

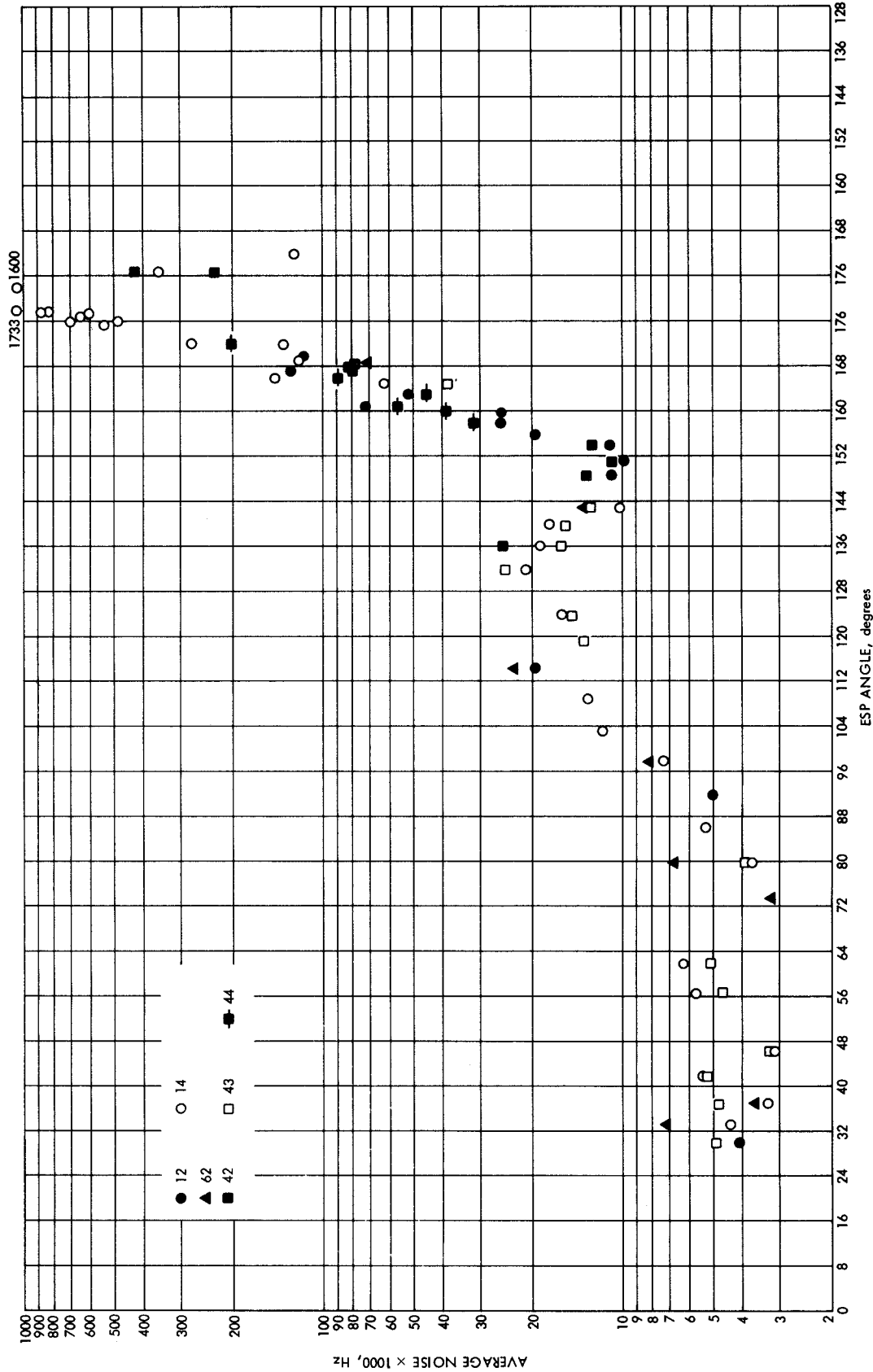


Fig. 6. Helios 1 average noise vs ESP angle

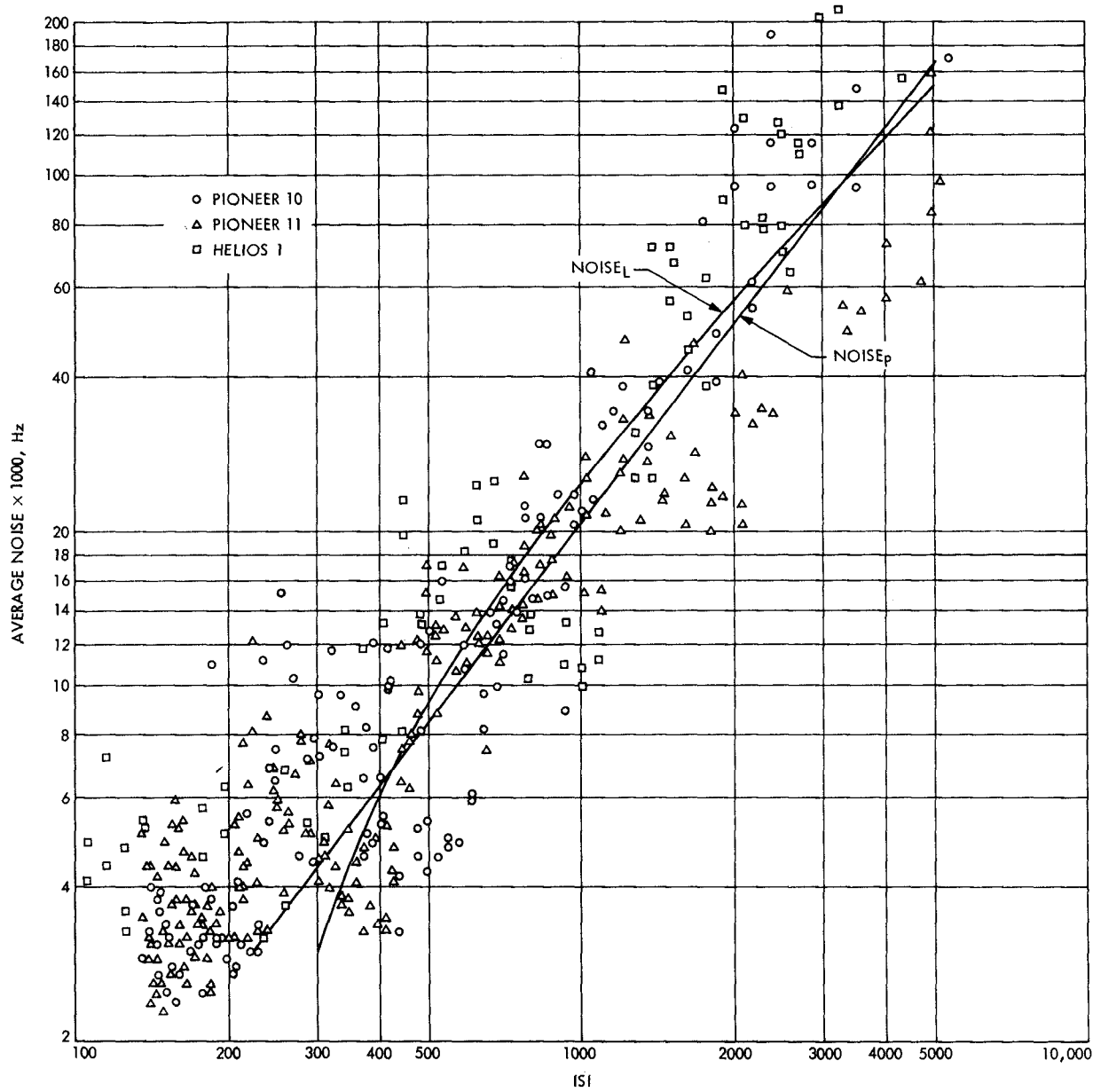


Fig. 7. Average noise vs ISI (mission composite)

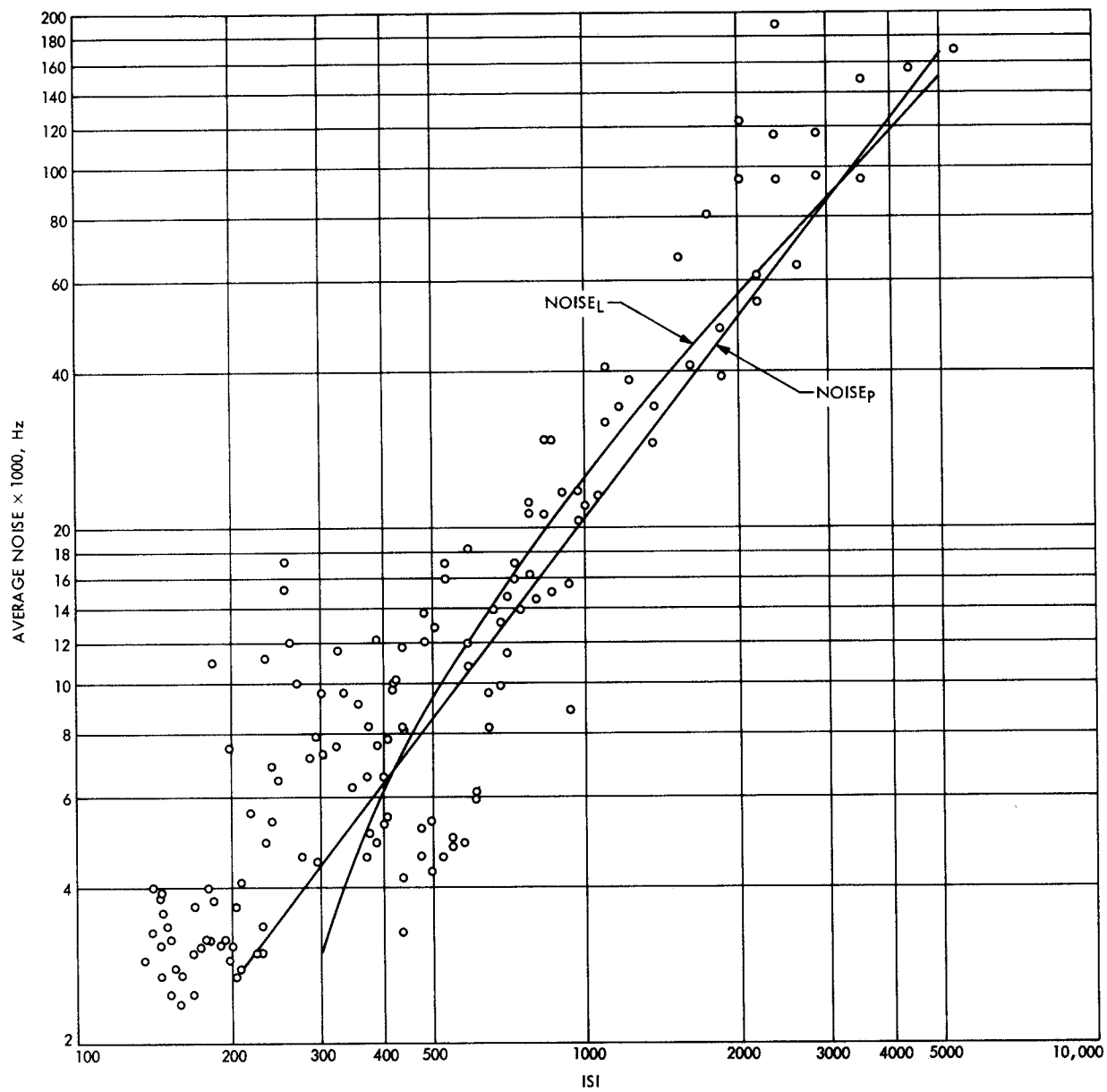


Fig. 8. Pioneer 10 average noise vs ISI

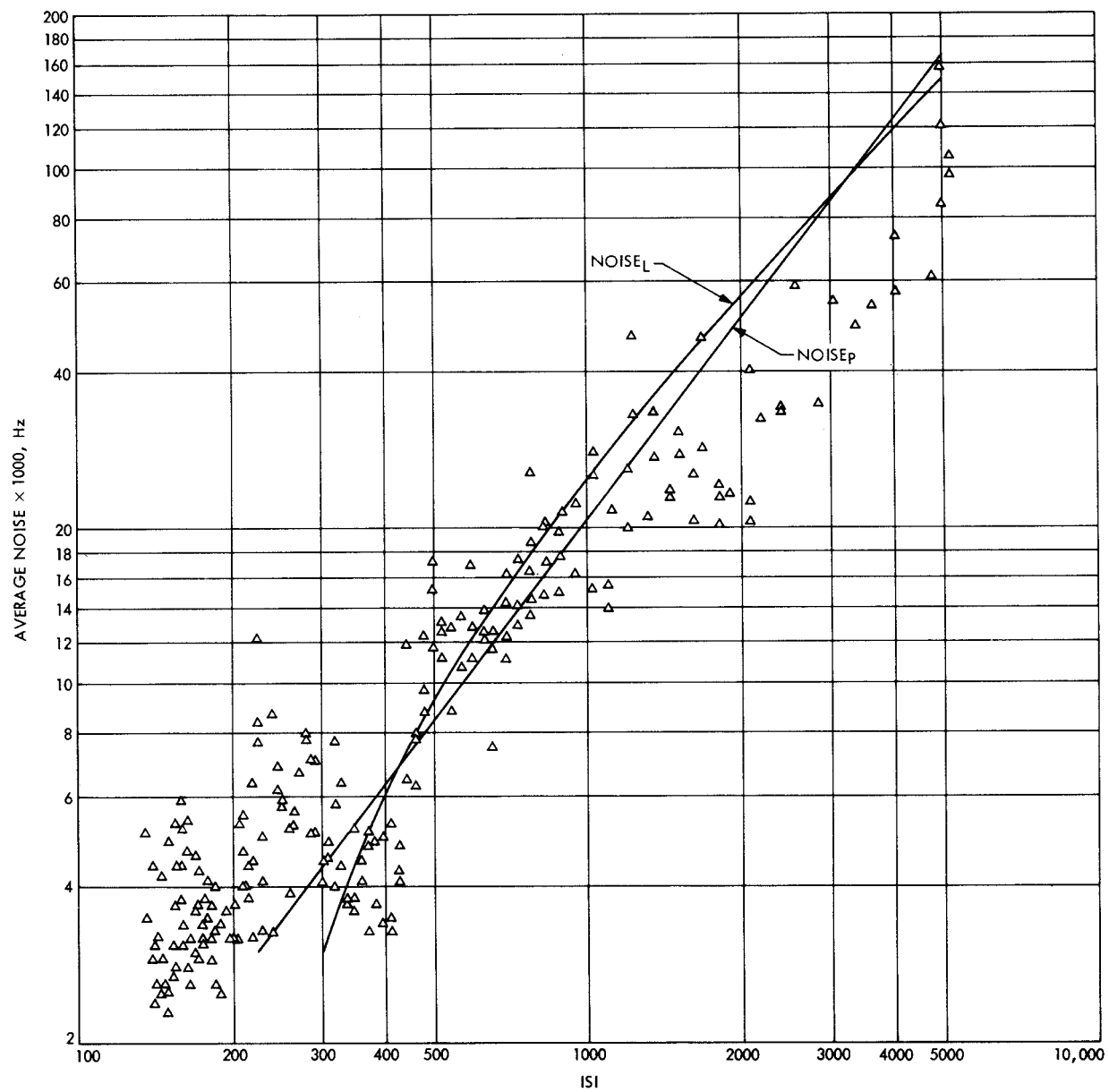


Fig. 9. Pioneer 11 average noise vs ISI

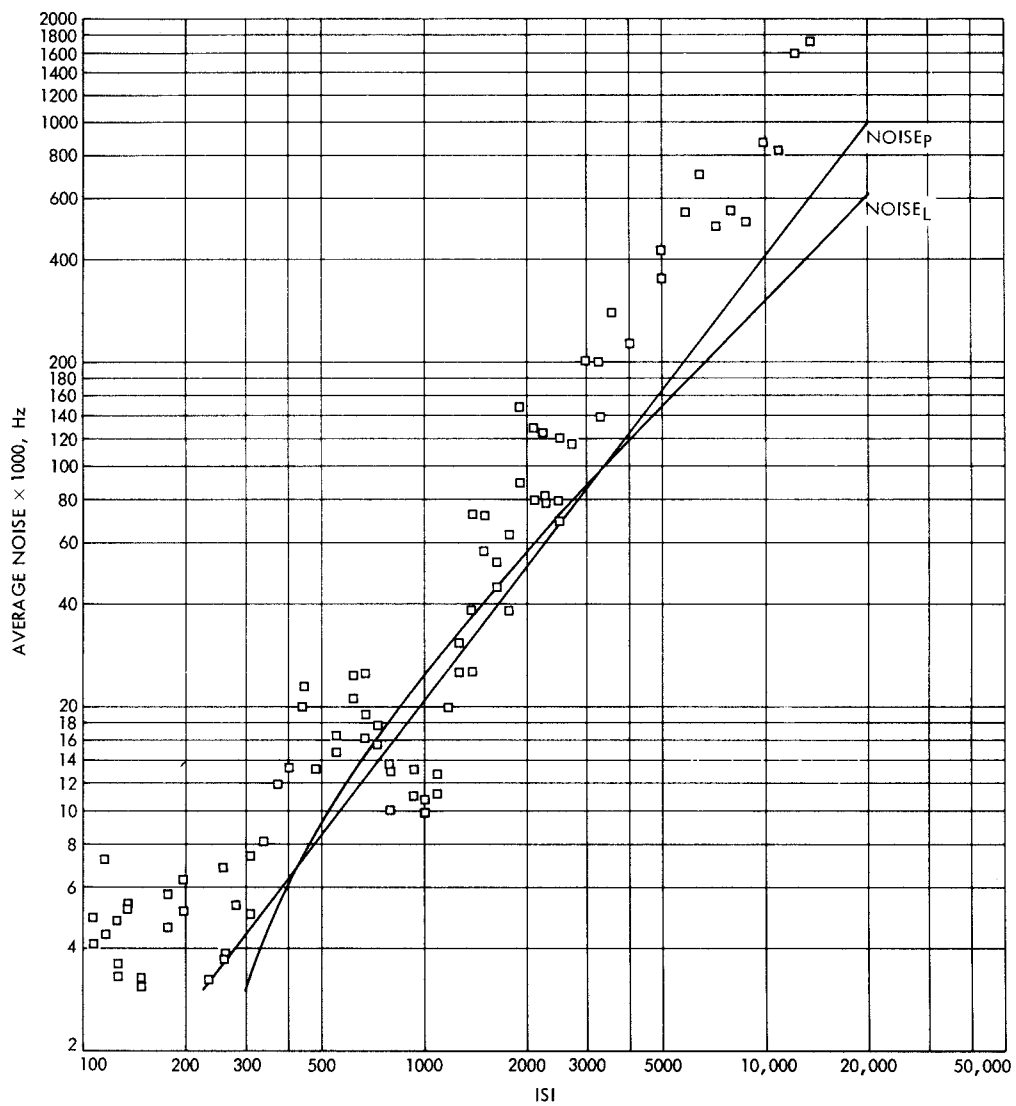


Fig. 10. Helios 1 average noise vs ISI

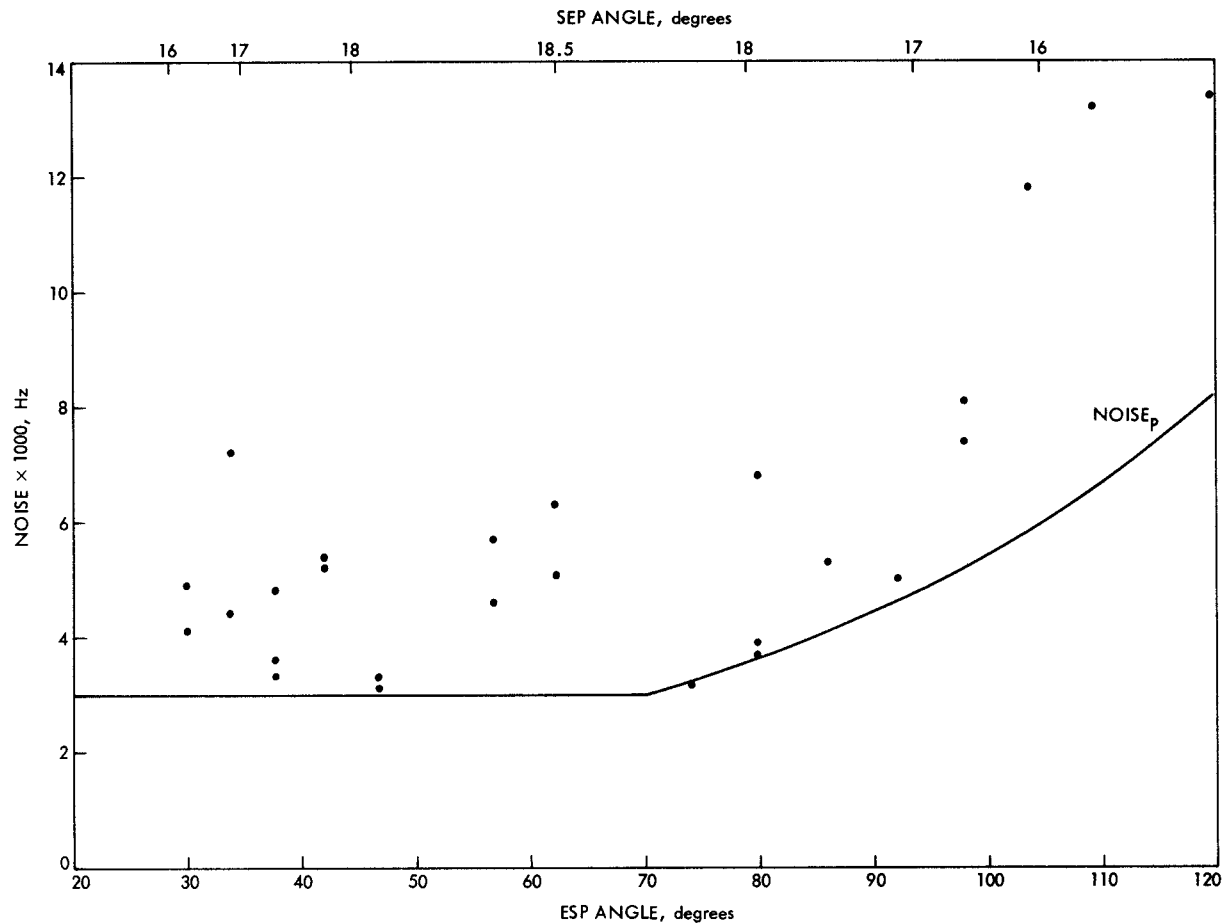


Fig. 11. Helios 1 perihelion: ESP vs average noise

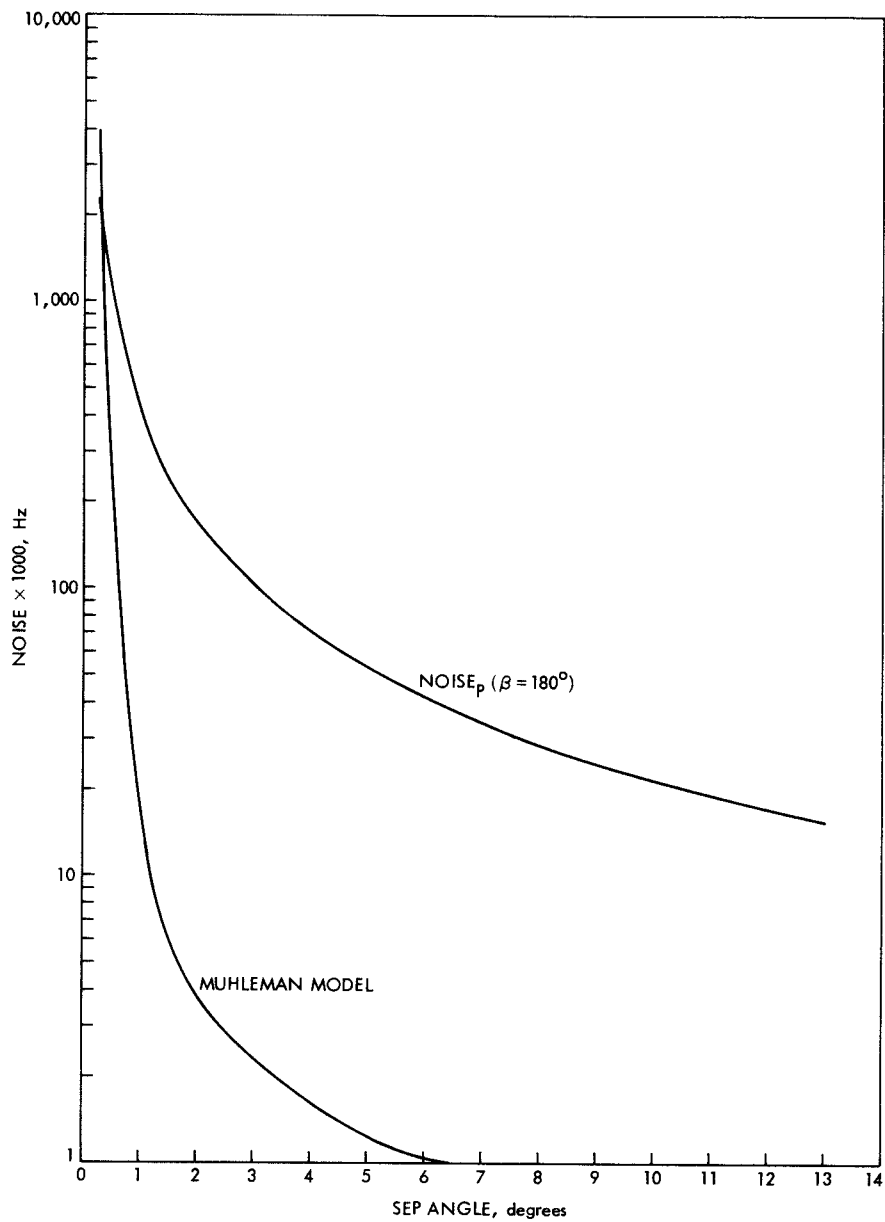


Fig. 12. Model comparison: average noise vs SEP angle